Experimental Investigation of the Governing Parameters in the Electrospinning of Poly(3-hydroxybutyrate) Scaffolds: Structural Characteristics of the Pores

Ashkan Heidarkhan Tehrani,[1] Ali Zadhoush,[1] Saeed Karbasi,[2] Saied Nouri Khorasani[3]

[1]*Department of Textile Engineering, Isfahan University of Technology, Isfahan 84156-83111, Iran*
[2]*Medical Physics and Biomedical Engineering Group, School of Medicine, Isfahan University of Medical Sciences, Isfahan 81746-73461, Iran*
[3]*Department of Chemical Engineering, Isfahan University of Technology, Isfahan 84156-83111, Iran*

Received 20 December 2009; accepted 12 April 2010
DOI 10.1002/app.32620
Published online 29 June 2010 in Wiley InterScience (www.interscience.wiley.com).

ABSTRACT: We sought to determine the impact of electrospinning parameters on a trustworthy criterion that could evidently improve the maximum applicability of fibrous scaffolds for tissue regeneration. We used an image analysis technique to elucidate the web permeability index (WPI) by modeling the formation of electrospun scaffolds. Poly(3-hydroxybutyrate) (P3HB) scaffolds were fabricated according to predetermined conditions of levels in a Taguchi orthogonal design. The material parameters were the polymer concentration, conductivity, and volatility of the solution. The processing parameters were the applied voltage and nozzle-to-collector distance. With a law to monitor the WPI values when the polymer concentration or the applied voltage was increased, the pore interconnectivity was decreased. The quality of the jet instability altered the pore numbers, areas, and other structural characteristics, all of which determined the scaffold porosity and aperture interconnectivity. An initial drastic increase was observed in the WPI values because of the chain entanglement phenomenon above a 6 wt % P3HB content. Although the solution mixture significantly ($p < 0.05$) changed the scaffold architectural characteristics as a function of the solution viscosity and surface tension, it had a minor impact on the WPI values. The solution mixture gained the third place of significance, and the distance was approved as the least important factor. © 2010 Wiley Periodicals, Inc. J Appl Polym Sci 118: 2682–2689, 2010

Key words: bioengineering; biopolymers; computer modeling; nanofiber

INTRODUCTION

The dream of not losing any failed organs may come true with the birth of an interdisciplinary field that applies both the principles of engineering and life science. Tissue engineering develops biological substitutions, in which tissue functions are restored and improved. Although there has been extensive research in many areas that would fall under the umbrella name of *tissue engineering*, it has always been a challenge for textile engineers to fulfill the need of producing an optimal fibrous structure that can mimic the extracellular matrix.[1–3]

Poly(3-hydroxybutyrate) (P3HB) is one of the most well-characterized homopolymers of the polyhydoxyalkanoate family, which are renowned for their desirable biocompatibility and biodegradability.[4–6] P3HB has long been used as surgical suture and in nerve repair, drug-delivery systems, and hard tissue repair.[7] With the presence of its monomeric component in the blood of healthy adults, P3HB was aptly chosen as a biomaterial for the fabrication of tissue scaffolds.[8]

Electric-field-driven fiber formation (electrospinning) has yet to be developed into a practical means for preparing novel porous structures with affordable mechanical properties.[1,9] Despite its relative ease of use, a multitude of processing parameters, such as the injection flow rate, applied voltage, and capillary-to-collector distance, can greatly affect the fiber formation and, consequently, the final structure.[10] The solution parameters, such as the viscosity and surface tension, and the volatility and conductivity are the other prominent factors that primarily affect the fluid-governing rheological behavior.[11] When fabricating an ideal fibrous scaffold, one should determine the effects of such important parameters on the pore architectural characteristics.

All scaffolds, regardless of their application, must meet a number of basic criteria to be applicable. At its most fundamental, a scaffold should not elicit an immune response while providing a viable framework for cellular infiltration and proliferation.[12] An

Correspondence to: A. Zadhoush (zadhoush@cc.iut.ac.ir).

© 2010 Wiley Periodicals, Inc.

ideal scaffold should have fine pores for maximum surface area and mechanical strength while having enough large and interconnecting apertures for blood vessel ingrowth.[13] What has often been challenging is the separate characterization of the scaffolds' pores and the investigation of their interconnectivity, instead of dependence only on the scaffold porosity.[14]

Methods used in the assessment of interconnectivity can hardly be quantitative when they are restricted to two-dimensional (2D) image microscopy.[15,16] Alternatively, they can be destructive, as in atomic force microscopy,[17] X-ray microtomography, and mercury intrusion porosimetry.[18] They cannot detect isolated pores in scaffolds, neither do they discriminate connections between pores in accordance to their diameters.[19] With such methods, previous studies have explored the relationship between the processing parameters and fiber diameter.[20] Nevertheless, none has elucidated the processing parameter effects on different pore characteristics.

In this study, to determine the effects of both the processing and material parameters of electrospinning on the pore interconnectivity, we simulated scaffold web formation with a unique image analysis approach. Aside from the common structural characteristics, web reconstruction was used to investigate the web permeability index (WPI), which can properly justify the pore interconnectivity of fibrous scaffolds. The impact of the electrospinning parameters on the scaffold porosity, pore number, and size of different fabricating conditions was gathered and analyzed. The results were used to explain how the jet formation and its spatial motion could alter these architectural characteristics. Eventually, the effects of the same parameters (control factors) on the WPI values (responses) were analyzed with the temperature and humidity assigned as noise factors in a Taguchi orthogonal design.

EXPERIMENTAL

Materials

P3HB [Chemical Abstract for Substance (CAS) = 26063-00-3; weight-average molecular weight = 300,000 g/mol] natural origin powder was purchased from Sigma-Aldrich (St. Louis, Missouri) and was used as received without further purification. Chloroform (CF) and dimethylformamide (DMF) were bought from Merck Germany.

Experimental design

A Taguchi L16 orthogonal array was designed with the help of Minitab 15.1.1.0 software (Minitab Inc., State College, Pennsylvania) to investigate the parameters' effects, four of which are renowned for their major influence on the architectural characteristic of resulting structures.[21] A conventional, full-factorial method of 64 runs was required to study these parameters. With the Taguchi design, they were reduced to 16 runs instead (Table I). Aside from the logic behind choosing the number of levels, their limits were confined in a way that the entire trial was processable.[11] For the sake of repeatability and signal-to-noise ratio analysis, each trial was carried out in three different noise conditions.

TABLE I
Plan of the Experiments

Run	A	B	C	D
1	1	1	1	1
2	1	2	1	1
3	1	3	2	2
4	1	4	2	2
5	2	1	1	2
6	2	2	1	2
7	2	3	2	1
8	2	4	2	1
9	3	1	2	1
10	3	2	2	1
11	3	3	1	2
12	3	4	1	2
13	4	1	2	2
14	4	2	2	2
15	4	3	1	1
16	4	4	1	1

Column A is the P3HB concentration, column B is the applied voltage, column C is the nozzle-to-collector distance, and column D is the solution mixture. They were determined with four, four, two, and two conditions per level, respectively.

Processing parameters

The electric field strengths for this certain polymer/solvent system was determined with four distinct values: 8, 10, 12, and 14 kV. In this range, the flow rate of the pump was always set in such a way that the jet initiated with a perfect cone. In this polymer/solvent system, a scaling law was developed between the applied voltage and the flow rate.[11] On the other hand, it was improper for the flow rate to be added as a separate control parameter because of its confounded interaction with the applied voltage.[10] The nozzle-to-collector distances were selected as 15 and 25 cm, for the least precedency.[22]

Material parameters

The polymer concentrations, which influence both the viscosity and the surface tension of the solution,[21] were selected as 6, 8, 10, and 12 wt %. For this range, the chain entanglement was assured, and proccessability within the other treatments was possible.[11] The solvent ratio had two distinct values, one with neat CF as the solvent and the second

TABLE II
Each Factor Level Assigned with a Specified Condition for Both the Processing and Material Parameters

Control factor	Level 1	2	3	4	Unit
Polymer concentration	6	8	10	12	wt %
Voltage	8	10	12	14	kV
Nozzle-to-collector distance	15	25	—	—	cm
Solution mixture	100 : 0	90 : 10	—	—	—

mixture with a proportion of 10% DMF as the cosolvent (Table II).

Electrospinning setup

A syringe pump used to force the solution (1 mL) through a small-diameter capillary (*i.d.* = 0.5 mm) to form a pendant drop at the tip. A positive electrode from a high-adjustable regulated power supply was then directly attached to the capillary, and a metal needle was used. A homemade collector was built to satisfy the need of fabricating a square dense three-dimensional (3D) scaffold for further image analyses. The collector's face was covered and isolated with a rubber film, except for a square 1 × 1 cm^2, where an aluminum sheet of the same size was placed for scaffolds to be collected without difficulty (Fig. 1).

Image analysis

The 16 scaffolds acquired from each one of the repetitions were mounted on a 4 × 4 cm^2 aluminum sheet and coated with gold in a BALTEC SCD 005 sputtering device (Gnathole Farm, Kettleshulme, High Peak, Cheshire SK23 7RE UK) for 3 min at 5 mA. The images were captured with a Philips XLS 30 series scanning electron microscope (The Netherlands) from six different arbitrary spots on each scaffold. All of the images had the same magnification of 750× and were captured with the same brightness and contrast to ease further image analysis.

Pore architectural characterization

After all of the images were cropped to the same size of 420 × 720 pixels, they were converted to binary mode with a well-defined threshold to reveal the surface layers of the scaffold.[3] Succeeding morphological operations enabled the removal of either the residual fibers in layers beneath or any unwanted noise. Pores were assumed as objects and labeled accordingly. For all of the images, the numbers of the open areas were counted, and their equivalent radius was computed. The porosity ($\bar{P}$) of each scaffold was computed as follows:

$$\bar{P} = \frac{1}{6}\sum_{i=1}^{6} P_i = \frac{1}{6}\sum_{i=1}^{6} \frac{a_{i1} + a_{i2} + \ldots + a_{in}}{A} = \frac{1}{6A}\sum_{i=1}^{6}\sum_{j=1}^{n} a_{ij} \quad (1)$$

where A is the total area where n voids were found and a_{ij} is the area of pore j found on image i of the same scaffold with a porosity of P_i.

For each scaffold, the successive repetition of the layers one on another simulated the actual structure of an electrospun scaffold. When a new layer was added, some open areas of the previous layers may have overlapped. As a result, a gradual reduction in the remaining open areas as a function of the deposited layers was derived; with x considered to be the number of layers; this is shown in eq. (2).

$$P_x = \left(\frac{\sum_{j=1}^{n} a_j}{A} \right)_x \quad (2)$$

where P_x is a discrete function in which x is its independent variable. P_x is the remaining open areas when x layers were deposited. To predict the nature of this relationship, an exponential curve was fitted on these discrete points with eq. (3):

$$F(x) = ae^{-bx} \quad (3)$$

where $F(x)$ is a continues function which represents the remaining accessible pores for x layers. a and b are constants.

Statistical analysis

The pore architectural characteristics were all analyzed with an SPSS 13.0 (SPSS Inc., an IBM Company, Chicago, Illinois) one-way analysis of variance. The simulation output data, the Taguchi responses,

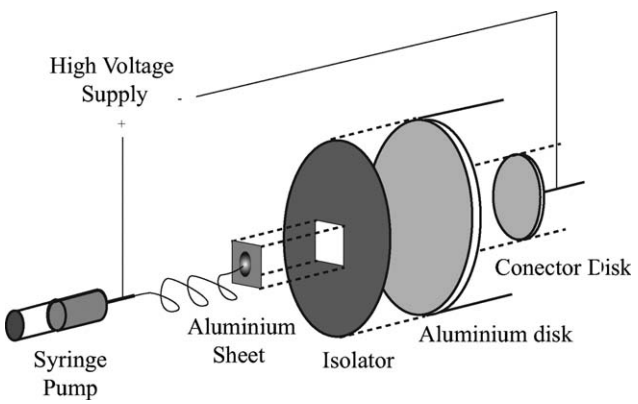

Figure 1 A circular aluminum sheet with a radius of 20 cm was used as a collector, not only to distribute the charge density uniformly but also to enable the accumulation of fibrous layers in its center.

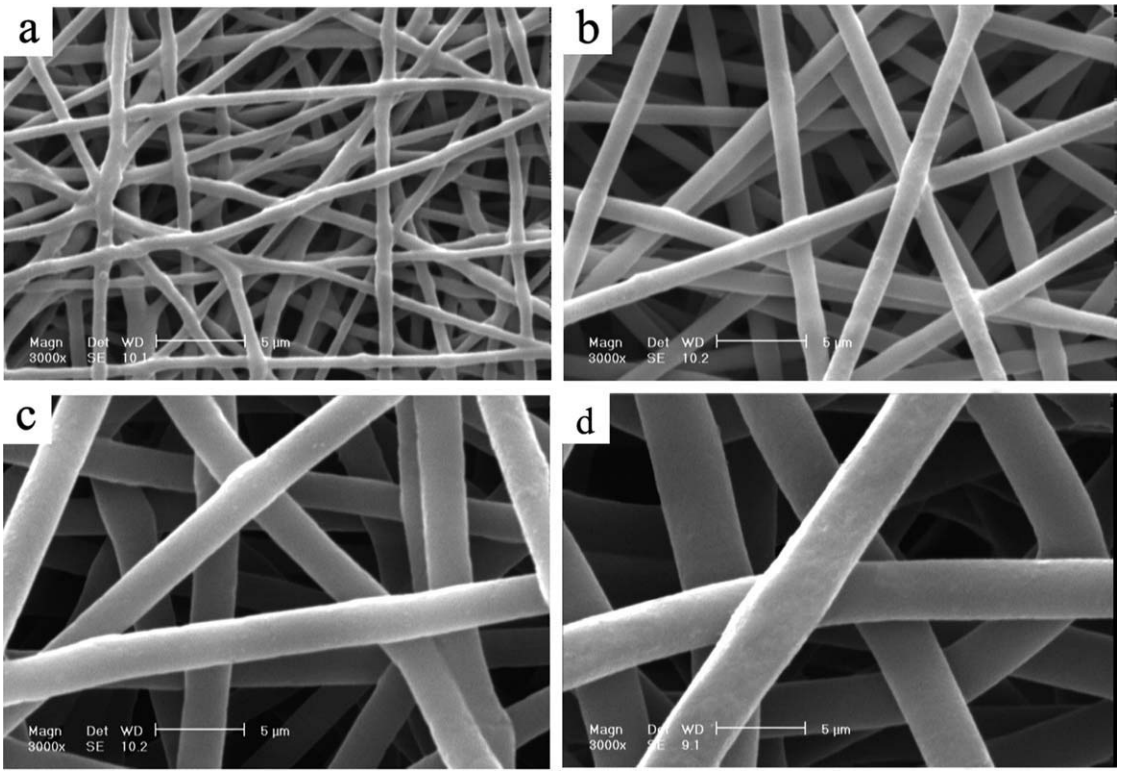

Figure 2 Smooth P3HB fibrous scaffolds without beads were obtained with diameters of approximately 700 nm to 4 μm. The selected specimens were fabricated with the following polymer concentrations, applied voltages, CF/DMF ratios, and distances, respectively: (a) 6 wt %, 12 kV, 100 : 0, and 25 cm; (b) 8 wt %, 8 kV, 100 : 0, and 25 cm; (c) 10 wt %, 14 kV, 100 : 0, and 15 cm; and (d) 12 wt %, 12 kV, 100 : 0, and 15 cm. A gradual increase in the fiber diameter due to higher polymer contents was observed.

were analyzed with both signal-to-noise ratios (smaller was better) and with analysis of means (ANOM) analysis in the Minitab 15.1 software. Through all these, p values less than 0.05 were considered to be statistically significant.

RESULTS AND DISCUSSION

We carried out all of the trails successfully, fabricating smooth P3HB electrospun fiber mats and justifying the selected conditions of levels for the L16 Taguchi experimental design (Fig. 2).

Porosity is considered for materials with a 3D structure, such as thick nonwoven fabrics.[23] On the same basis, for a 2D layer, the fraction of open areas proportional to the total area of the same layer is considered as porosity.[24] Because of the selected threshold, the layer thickness was considered to be negligible, as with a 2D structure.[3] Assuming that the fibers diameter in a layer was equal to the layer thickness itself, we reconstructed the 3D virtual structure by their random successive repetition (Fig. 3). The exponential relationship between the number of layers built up and the remaining open areas was obtained with 95% confidence bounds ($R^2 = 0.999$).

The first derivation of the fitted curve [eq. (3)] was the rate in which the dead-end channels appeared. This rate reached its minimum where the accessibility to the inner pores of the following layers became impossible. For an ideal scaffold, one needs an infinite number of layers build up to lose the interconnectivity. This was explained by the mathematically driven eq. (4):

$$\lim_{x\to\infty} \frac{dF(x)}{dx} = 0 \Rightarrow P_{x\to\infty} = \left(\frac{\sum_{j=1}^{n} a_j}{A} \right)_{x\to\infty} = 0 \quad (4)$$

According to eqs. (3) and (4), the absolute value of the constant b can determine how fast the addition of new layers may block the entrance of a channel [eq. (5)]:

$$\frac{dF(x)}{dx} = -abe^{-bx} \quad (5)$$

The exponent b can truly measure the interconnectivity of the pores within a fibrous scaffold. The congestion of the overlapped layers altered the web structure and developed each a particular WPI. The permeability changes were reflected in the value of b. The greater the b became, the faster the dead-end

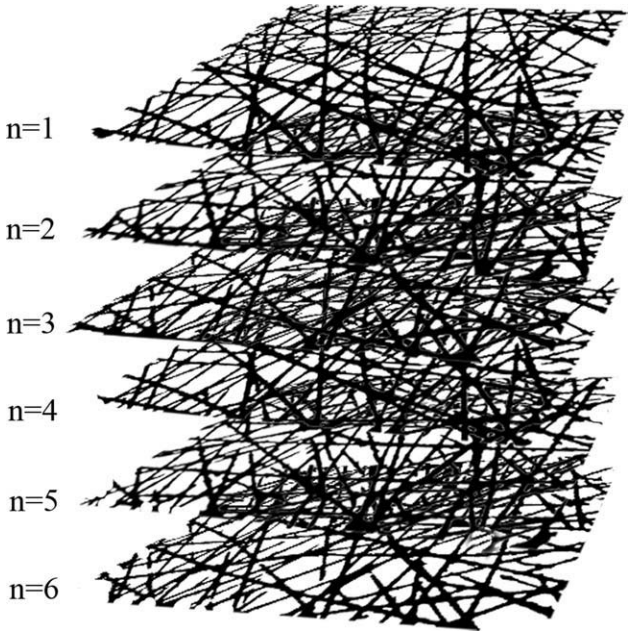

Figure 3 3D reconstructed fibrous scaffold with $n = 6$ deposited random layers, all of which were obtained from a single specimen with a polymer concentration of 8 wt %, 12 kV of applied voltage, and neat CF at a nozzle distance of 25 cm from the collector.

channels appeared. As a result, for any electrospun scaffold with a lower WPI, greater pore interconnectivity was expected. The scaffold WPI values, which were determined in three different noise condition (repeats), are presented in Table III.

TABLE III
Sixteen Taguchi Runs and Their Resulting WPIs, R_1, R_2, and R_3, as the Responses that Were Presented in Three Repetitions of Noise Conditions

Run No.	R_1	R_2	R_3
1	0.528	0.504	0.518
2	0.496	0.512	0.516
3	0.493	0.533	0.513
4	0.611	0.616	0.605
5	0.631	0.607	0.598
6	0.609	0.618	0.609
7	0.598	0.612	0.615
8	0.714	0.716	0.700
9	0.599	0.805	0.605
10	0.600	0.603	0.638
11	0.633	0.618	0.572
12	0.593	0.598	0.626
13	0.611	0.622	0.607
14	0.610	0.607	0.601
15	0.614	0.603	0.618
16	0.811	0.780	0.778

Polymer concentration

With increasing polymer concentration, the WPIs increased and showed a reduction in the scaffold pore interconnectivity. The solution viscosity increased when the polymer content was built up. These conditions caused the fibers to become thicker and their distribution to get narrower.[1,25,26] From the analysis of variance, the same happened when the numbers of pores were reduced and both the mean pore size and the scaffold porosity increased (Table IV). For any aperture of a fibrous layer with fewer pores, the chance of overlapping with an opening of another deposited layer becomes less probable. Therefore, the inner apertures were blocked faster when a more viscous solution was used.

The prominent factor that alters pore characteristics, such as their number and areas, is definitely triggered from where the polymeric solution jet forms.[10,22] After the jet forms, its stability and whipping motion

TABLE IV
Analyses of Variance for the Pore Architectural Characteristic of the Fibrous Scaffolds when the Processing and Materials Parameters of the Electrospinning Were Altered

		Polymer concentration	Applied voltage	Trajectory distance	Solution mixture
Porosity	SSE	117.95	39.53	12.27	48.49
	MSE	39.32	13.18	12.27	48.49
	DOF	3	3	1	1
	F	4.73	0.89	1.13	4.30
	P	0.02	0.47	0.30	0.05
Pore number	SSE	183942.69	40,863.18	35,250.06	330,050.25
	MSE	61,314.23	13,621.06	35,250.06	330,050.25
	DOF	3	3	1	1
	F	1.85	0.23	0.70	14.01
	P	0.19	0.87	0.41	0.00
Mean pore size	SSE	3,424,775.72	500,804.05	465,443.71	5,957,176.64
	MSE	1,141,591.91	166,934.69	465,443.71	5,957,176.64
	DOF	3	3	1	1
	F	2.07	0.22	0.68	24.51
	P	0.15	0.89	0.42	0.00

SSE = sum of squares of error; MSE = mean of squares of error; DF = degrees of freedom; F = F-statistic is a ratio of the mean square error of the factor and the mean square error.

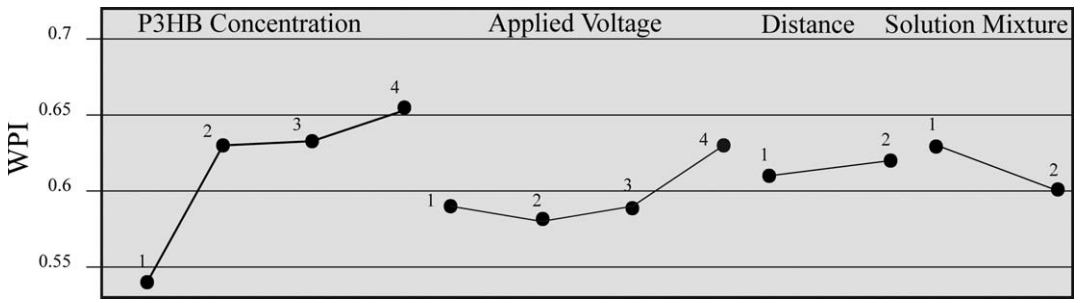

Figure 4 Taguchi mean effect analysis of the WPI values. A dramatic increase from 6 to 8 wt % of P3HB was remarkable. An initial improvement in the pore interconnectivity due to WPI elevation when the voltage was increased from 8 to 10 kV was noticeable.

magnitude determines the final structural properties. Shin et al.[27] suggested a model for jet stability as a function of fluid properties, in which the solution viscosity was considered as one of the most significant variables.

A higher degree of chain entanglement, due to higher viscosities, makes it harder for the electrostatic force to drag and extend individual chains.[28] Therefore, the longer stability of the ejected charged jet leads to fewer numbers of pores and thicker bridges.[29] For more, it is probable for the upper layers to overlap the pores of the layer beneath, and a greater reduction is expected in pore interconnectivity. This became crystal clear when a dramatic increase occurred when the solution was concentrated above a 6 wt % P3HB content (Fig. 4). According to the Taguchi analysis, the viscosity had the greatest impact on the WPIs and was considered significant (Table V).

Applied voltage

The effect of the applied voltage seemed to be feeble when it came to the pore characteristics. Although when a higher electrostatic force was applied proportional to higher flow rates, the WPI values increased with significant importance (Fig. 4). Vividly, when a greater number of smaller apertures or fewer numbers of larger ones are produced, it is reasonable to judge that the porosity would not change in an ideal situation.[22] The same argument was used when no meaningful relationship was observed between the applied voltage and the scaffold porosity (Table IV).

Fundamentally, for a given nozzle-to-collector distance, there is a close relationship between the adjusted flow rate and the applied voltage.[30] A voltage lower than a minimum yields a dripping mode because of an insufficient supply of solution to the cone, whereas a voltage higher than a maximum accounts for the contraction of the cone.[11]

Now within these safety boundaries, dragging the chains more vigorously by increasing the electrostatic force (higher mass delivery from the cone), we had thinner fibers and, as a result, larger pores and, as discussed previously, better interconnections.[10] However, this was reported to be reversed because of highly charged jet dramatic whipping motions. After the initial tinning, there was a monotonical increase in the fiber diameter. Because of what happens for more viscous solutions, this lessened the chance of pore accessibility to one another and caused the pore interconnectivity to decrease afterward. This explained the initial disobedience of the WPI increasing relationship with applied voltage. According to the Taguchi analysis, the applied voltage had the second priority in controlling the WPIs and was considered significant (Table V).

TABLE V
Taguchi Analysis of the Signal-to-Noise Ratio and Mean Effects for the Electrospinning Parameters

		Signal-to-noise ratio					Mean			
Source	DF	Sequential SS	Adjusted MS	*F*	*p*	DF	Sequential SS	Adjusted MS	*F*	*p*
A	3	6.9328	2.31093	7.82	0.012	3	327.043	109.014	5.75	0.026
B	3	4.4485	1.48283	5.02	0.036	3	240.842	80.281	4.23	0.053
C	1	0.0971	0.09707	0.33	0.585	1	4.134	4.134	0.22	0.655
D	1	0.4645	0.46451	1.57	0.250	1	38.234	38.234	2.02	0.199

The influences of polymer concentration (A) and applied voltage (B) on the WPI values were both considered significant ($p < 0.05$). The nozzle-to-collector distance (C) and the solution mixture (D) were determined to be insignificant. DF = degrees of freedom; SS = sum of squares; MS = mean of squares; F = F-statistic is a ratio of the mean square error of the factor and the mean square error.

TABLE VI
Rank of All Input Factors Representing Their Relative Impact on WPI and, Consequently, on the Pore Interconnectivity for the Electrospun Fibrous Scaffolds

	Signal-to-noise ratio				Mean			
Factor level	A	B	C	D	A	B	C	D
1	34.57	35.51	35.60	35.85	53.71	60.29	60.79	62.85
2	36.04	35.31	35.76	35.51	63.56	58.49	61.81	59.75
3	35.83	35.31	—	—	62.42	58.52	—	—
4	36.27	36.58	—	—	65.52	67.90	—	—
Δ	1.70	1.27	0.16	0.34	11.81	9.41	1.02	3.09
Rank	1	2	4	3	1	2	4	3

Δ statistics, which compare the relative magnitude of the effects, grouped them in the following order of importance: Polymer concentration > Applied voltage > Solution mixture > Nozzle-to-collector distance.

Solution mixture

For the CF/DMF system, the WPIs and pore mean size decreased, but the pore numbers increased in comparison to the neat CF system. On the other hand, the porosity decreased. This showed that the mean area reduction dominated for less volatile but more conductive mixtures. The effects of the solution properties earned the third rank according to the Taguchi analysis (Table VI).

CF had a lower dielectric constant (~ 4.8) and conductivity (<0.1 μS/cm) in comparison with the DMF solvent (36.7 and 0.6 μS/cm, respectively).[11] However, because of the more volatile nature of the neat CF in contrast to the CF/DMF cosolvent, severe stretching of P3HB jets before polymer solidification was hindered in the former system. That being the case, a thicker jet allowed less whipping instability and, finally, produced larger but fewer numbers of pores. The outcome was compact layers of fewer interconnected channels.

The CF/DMF system could be considered from another point of view, in which the solution viscosity decreased because of the poor affinity of DMF molecules to the P3HB chains and resulted in an increase in the surface tension and the solution conductivity. The presence of the ions increased the capacity of the charge delivery in a less viscous jet and, thereby, subjected it to higher tension, and the result was a denser layer with a considerably small size but a greater number of pores; a similar result was obtained when a higher electrostatic drag force was applied. This could have explained why there were more interconnected pores in a less volatile but more conductive system.

Distance

Distance was hypothesized to have the least impact on the response. With that in mind, it was rational to conclude that the further the stationary collector was placed, the larger the whipping jet became. In this situation, the outcome was definitely a web with more oriented fibers, pores with a consistent geometry, and probably fewer interconnected channels. Although increasing the space between the nozzle and the collector reduced the electric intensity adjacent to the collector, statistics analyses suggested that, despite it being an insignificant factor, a minimum value was still required to allow sufficient solvent evaporation, particularly in the bending instability region.[11]

CONCLUSIONS

In this research, the electrospun WPI was defined as a criterion to quantitatively determine fibrous scaffold pore interconnectivity. Image analysis of the 3D reconstructed fibrous scaffolds helped us to quantify their architectural characteristics, such as their pore numbers, pore size, and scaffold porosity. WPI values were assigned as the responses when the electrospinning parameters were altered according to a Taguchi design. With the response analysis, they were ranked from the most significant one to the least important in the following order: Polymer concentration < Applied voltage < Solution mixture < Nozzle-to-collector distance. The jet stability was held responsible for the resulting structural characteristics of the webs. The scaffold pore interconnectivity was reduced when a more viscous solution was used. Increasing the applied voltage initially enhanced the pore interconnectivity, which was then steadily reduced. Any variation when levels of the other parameters were changed seemed relatively small. Accurate control over the web structure is, therefore, essential for measuring the scaffold applicability to guarantee the ingress of large numbers of cells and to allow the formation of cellular associations. An *in vitro* evaluation could result in a better understanding of how the pore architectural characteristics may influence such a biological mechanism.

Our future goal is to investigate the agreement of the simulation-deduced criterion with the cell viability on the same scaffolds, the results of which will be published in the near future.

References

1. Sill, T. J.; von Recum, H. A. Biomaterials 2008, 29, 1989.
2. Ghasemi-Mobarakeh, L.; Prabhakaran, M. P.; Morshed, M.; Nasr-Esfahani, M.-H.; Ramakrishna, S. Biomaterials 2008, 29, 4532.
3. Ghasemi-Mobarakeh, L.; Semnaniand, D.; Morshed, M. J Appl Polym Sci 2007, 106, 2536.
4. Zhao, K.; Deng, Y.; Chen, J. C.; Chen, G.-Q. Biomaterials 2003, 24, 1041.
5. Zhang, L.; Zheng, Z.; Xi, J.; Gao, Y.; Ao, Q.; Gong, Y.; Zhaoand, N.; Zhang, X. Eur Polym J 2007, 43, 2975.
6. Gao, Y.; Kong, L.; Zhang, L.; Gong, Y.; Chen, G.; Zhaoand, N.; Zhang, X. Eur Polym J 2006, 42, 764.
7. Hazerand, B.; Steinbüchel, A. Appl Microbiol Biotechnol 2007, 74, 1.
8. Li, X.-T.; Zhangand, Y.; Chen, G.-Q. Biomaterials 2008, 29, 3720.
9. Agarwal, S.; Wendorffand, J. H.; Greiner, A. Polymer 2008, 49, 5603.
10. Subbiah, T.; Bhat, G. S.; Tock, R. W.; Parameswaran, S.; Ramkumar, S. S. J Appl Polym Sci 2005, 96, 557.
11. Wang, C.; Hsuand, C.-H.; Hwang, I.-H. Polymer 2008, 49, 4188.
12. Sell, S.; Barnes, C.; Simpson, D.; Bowlin, G. J Biomed Mater Res Part A 2007, 85, 115.
13. Atwood, R. C.; Jones, J. R.; Lee, P. D.; Hench, L. L. Scr Mater 2004, 51, 1029.
14. Laurenci, C. T.; Nair, L. S. Nanotechnology and Tissue Engineering: The Scaffold; CRC Taylor & Francis: New York, 2008.
15. Ziabari, M.; Mottaghitalab, V.; Haghi, A. K. Korean J Chem Eng 2008, 25, 905.
16. Ziabari, M.; Mottaghitalab, V.; McGovern, S. T.; Haghi, A. K. Nanoscale Res Lett 2007, 2, 597.
17. Safinia, L.; Mantalaris, A.; Bismarck, A. Langmuir 2006, 22, 3235.
18. Moore, M. J.; Jabbari, E.; Ritman, E. L.; Lu, L.; Currier, B. L.; Windebank, A. J.; Yaszemski, M. J. J Biomed Mater Res Part A 2004, 71, 258.
19. Safinia, L.; Mantalaris, A.; Bismarck, A. Langmuir 2005, 22, 3235.
20. Heikkila, P.; Harlin, A. Eur Polym J 2008, 44, 3067.
21. Helgeson, M. E.; Grammatikos, K. N.; Deitzel, J. M.; Wagner, N. J. Polymer 2008, 49, 2924.
22. Reneker, D. H.; Yarin, A. L. Polymer 2008, 49, 2387.
23. Dierickx, W. Geotext Geomembr 1999, 17, 231.
24. Ziabari, M.; Mottaghitalab, V.; Haghi, A. K. Korean J Chem Eng 2008, 25, 919.
25. Huang, Z.-M.; Zhang, Y.-Z.; Kotaki, M.; Ramakrishna, S. Compos Sci Technol 2003, 63, 2223.
26. Rutledge, G. C.; Fridrikh, S. V. Adv Drug Delivery Rev 2007, 59, 1384.
27. Shin, Y. M.; Hohman, M. M.; Brenner, M. P.; Rutledge, G. C. Appl Phys Let 2001, 78, 1149.
28. Ying, T. H.; Ishii, D.; Mahara, A.; Murakami, S.; Yamaoka, T.; Sudesh, K.; Samian, R.; Fujita, M.; Maeda, M.; Iwata, T. Biomaterials 2008, 29, 1307.
29. Sombatmankhong, K.; Sanchavanakit, N.; Pavasant, P.; Supaphol, P. Polymer 2007, 48, 1419.
30. Frenotand, A.; Chronakis, I. Curr Opin Colloid Interface Sci 2003, 8, 64.